Fault-Tolerant Control of a Triple Redundant PMA-SynRM Driven Under Single-Phase Open-Circuit by Mono-Inverter

Meiling Zhao, Guohai Liu, *Senior Member, IEEE*, Qian Chen, *Senior Member, IEEE*, Wenxiang Zhao, *Senior Member, IEEE*, and Christopher H. T. Lee, *Senior Member, IEEE*

***Abstract*—In this article, a new fault-tolerant control strategy for a triple redundant 3 × 3 phase permanent magnet assisted synchronous reluctance motor under a single-phase open-circuit fault has been proposed. In order to reduce the cost of the system, a two-level three-phase inverter is constructed to drive the parallel-connected motor under normal and fault-tolerant conditions. In normal operations, the current and torque are equally distributed to the three modules of the motor, while in a fault-tolerant state, they should be redistributed according to a specific ratio. The optimal ratio is obtained by investigating the control strategy of minimum copper loss and minimum torque ripple. The torque ripple of the normal module is increased to offset the torque ripple of the fault module, thereby reducing the total electromagnetic torque ripple after the failure. It means that no auxiliary switching devices need to be added even if the failure happened, which can significantly reduce the complexity and improve the reliability of the control system. To verify the theoretical analysis, simulations and experiments have been conducted. The results are in good agreement with that of theoretical analysis.**

***Index Terms*—Copper loss, fault-tolerant, mono-inverter, torque ripple.**

I. Introduction

MULTIPHASE permanent magnet (PM) assisted synchronous reluctance motor (PMA-SynRM) has been widely used in aerospace actuation, transportation areas, owing to the merits of high efficiency, high power density, less torque ripple and improved fault-tolerant capability [1]–[4]. However, with the increase of motor phase numbers, more power electronic devices need to be added, which will increase the cost and the volume of the control system. To reduce the cost and expand the application, the mono inverter parallel drive system has been a hot topic in research [5]–[13].

Some researchers focus on using the mono inverter to drive two motors, which have different drive shafts [5]–[7]. Owing to the unequal load torque of these two motors, the master-slave technique is adopted, that is to say, the motor with a higher load is the master motor, which adopts closed-loop control, while the slave motor adopts open-loop control. The performance of the control system is fully dependent on the parameters of the motor [8]. To reduce the dependence of the control system on motor parameters, a new variable related to the load can be introduced [9]. Besides, weight vector control is proposed to improve the performance of the control system under unbalanced torque [10]. In general, the previous researches on the mono inverter control system mainly focus on reducing loss [11], ensuring parameter independence [12], and improving torque performance under different loads [13]. However, motors in the above studies are all operated under normal conditions, and the mono-inverter drive control after the failure has not been considered.

In the fields of aerospace, rail transportation and electric vehicle [14], the reliability requirements of motors are high. Since open-circuit faults account for 21%–37% of motor failures [15], the research on open-circuit fault-tolerant control (FTC) has a great significance. Open-circuit fault includes inverter fault and winding fault. For three-phase PMSM, when one phase of the motor or one leg of the inverter fails, the method of redundancy bridge arm can be used to realize the FTC to ensure smooth operation [16]. If a fault occurs in two legs of the inverter, the motor will stop working. However, the probability of an open-circuit fault occurring simultaneously in two legs of the inverter is low [17]. Compared with the three-phase motor, the multiphase motor has more control degrees of freedom. After the winding open-circuit fault occurs, the undisturbed fault-tolerant operation can be realized without adding additional hardware circuits.

The research on FTC for winding open-circuit fault can be mainly divided into three categories, namely optimal torque control [18], [19], unchanged magnetomotive force (MMF) control [20], [21], and reduced-order decoupling control [22]–[25]. The control objectives of FTC include minimum copper loss, smooth output torque and maximum average torque [18]–[20].

Manuscript received July 11, 2020; revised November 8, 2020 and January 21, 2021; accepted March 14, 2021. Date of publication March 17, 2021; date of current version June 30, 2021. This work was supported in part by the National Natural Science Foundation of China under Grants 51877098 and 52077097, in part by the Natural Science Research Project of Higher Education Institutions of Jiangsu Province under Grant 20KJA470003, and in part by the Priority Academic Program Development of Jiangsu Higher Education Institutions. Recommended for publication by Associate Editor S.-C. Yang. *(Corresponding author: Qian Chen.)*

The authors are with the School of Electrical and Information Engineering, Jiangsu University, Zhenjiang 212013, China, and also with the Jiangsu Key Laboratory of Drive and Intelligent Control for Electric Vehicle, Zhenjiang 212013, China (e-mail: 2111907003@stmail.ujs.edu.cn; ghliu@ujs.edu.cn; chenqian0501@ujs.edu.cn; zwx@ujs.edu.cn; Chtlee@ntu.edu.sg).

Color versions of one or more figures in this article are available at https://doi.org/10.1109/TPEL.2021.3066797.

Digital Object Identifier 10.1109/TPEL.2021.3066797

An unchanged MMF method is proposed to reduce torque ripple when one phase opens [21]. Nevertheless, a hysteresis current controller is used in this control strategy, which will increase the switching frequency of the inverter, thus increasing the loss of the whole control system. In addition, redistribution of torque after the failure has been introduced in [26]. However, the above control objects are limited to the surface PMSM, whose electromagnetic torque can be controlled by the current in the q-axis, directly, and reluctance torque is ignored. For the PMA-SynRMs, the cross-coupling effect can be significantly improved in MMF and the optimal torque has been researched in [27]. In [28], different kinds of the fault of 3 × 3 phase PMA-SynRMs have been analyzed. In general, when one phase is disconnected, the corresponding module will be isolated. It means that the electromagnetic torque is only provided by the other two modules. Therefore, the amplitude of the phase current will be increased significantly to ensure the output torque. Besides, FTC of five-phase flux switched PMSM, which has reluctance torque, was considered in [29]. However, the intellectual algorithm is used to reduce the torque ripple instead of making full use of reluctance torque. At present, most of the FTCs of multiphase motor focus on the improvement of control algorithms driven by multiple inverters [18]–[29]. There are few studies on FTC driven by mono-inverter, which can significantly reduce the complexity of the control system [15], [30]. However, in these mono-inverter drives for fault-tolerant operation, the reluctance torque is not considered, which is hard to apply into PMA-SynRMs.

In this article, a new FTC strategy is proposed for a triple redundant 3 × 3 phase PMA-SynRM under a single-phase open-circuit fault. The contribution of this article comes from the following.

1) Mono-inverter is constructed to drive the parallel-connected motor under normal and fault-tolerant conditions. Compared with the traditional three two-level three-phase inverters driving a 3 × 3-phase motor, the proposed method eliminates two two-level three-phase inverters and hardware circuits. In addition, with the decrease of the leg of the inverter, the possibility of inverter fault will also be reduced. Therefore, the method can significantly improve the cost-effectiveness and reliability of the control system.
2) When the motor has an open-circuit fault, not only the healthy windings provide the output torque, but also the remaining two phases of the faulty module participate in the electromechanical energy conversion. By redistributing the torque of each module after fault, the stator current can be obtained to minimize copper loss and torque ripple.

This article is organized as follows: the triple redundant 3 × 3 phase PMA-SynRM and its driving system are introduced in Section II. In Section III, two operation modes are analyzed. Based on the current in the static coordinate system, the torque distribution in normal and fault-tolerant states is analyzed. Besides, the minimum copper loss and minimum torque ripple are regarded as restrictive conditions to redistribute the reluctance torque after failure. The controllability and operating capability of the FTC system are also presented in this section. Moreover, the control system is described in detail in Section IV.

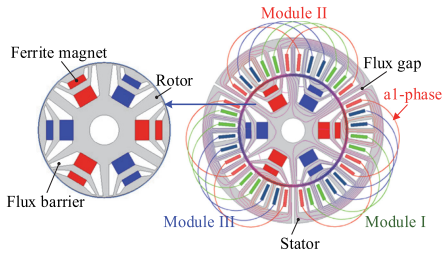

Fig. 1. Cross-section of 3 × 3 phase PMA-SynRM.

TABLE I
SELF AND MUTUAL INDUCTION OF 3 × 3 PHASE PMA-SYNRM

L_{a1a1}	13.4 mH	L_{a1b1}	-4.83 mH	L_{a1c1}	-4.98 mH
L_{a1a2}	0.17 mH	L_{a1b2}	-0.1 mH	L_{a1c2}	-0.002mH
L_{a1a3}	0.25 mH	L_{a1b3}	0.04 mH	L_{a1c3}	-0.21 mH

Simulation and experimental results are accomplished in Section V to verify the FTC strategy. Finally, the conclusion is drawn in Section VI.

II. TRIPLE REDUNDANT MODULAR PMA-SYNRM AND DRIVE

The cross-section of triple redundant 3 × 3 phase PMA-SynRM is shown in Fig. 1. It can be seen that the stator is composed of three modules. Each module has 12 armature slots. The armature winding in each module is separated into three phases. In the rotor, two levels flux barriers are adopted, and ferrite magnets are inserted in the flux barriers.

Besides, the flux linkage generated by the armature reaction of the motor is also illustrated in Fig. 1. Due to the design of the flux gap structure, the flux linkage forms a loop in the stator module through the rotor, rather than in series with other modules. Besides, the mutual inductances between a1-phase winding and the other eight phases are given in Table I. It can be found that the maximum ratio of self-inductance and mutual inductance, namely La1a3/La1a1 is just about 1.86%. Therefore, the influence of the fault module on other normal modules can be ignored. It means that modular design promotes the inherent fault-tolerant performance to achieve electrical, magnetic, thermal, and physical isolation.

It should be noted that the motor is a symmetrical-type motor with three three-phase windings whose phases are aligned. The phases of this studied 3 × 3 phase motor can be, respectively, defined as phase-a1, phase-b1, phase-c1 in module I, phase-a2, phase-b2, phase-c2 in module II, and phase-a3, phase-b3, phase-c3 in module III. The three modules can be approximately equivalent to three three-phase motors. For the sake of simplicity, assume that the three modules share the same parameters.

In the traditional control method, three two-level three-phase inverters are adopted to drive the three modules independently, which will increase the cost of the drive circuit [31]. To reduce the total volume, weight and cost of the system, a control method with parallel-connection is proposed, which is depicted in Fig. 2. As can be observed, voltage is shared among the three modules and each module has an independent neutral point (n_1, n_2, n_3).

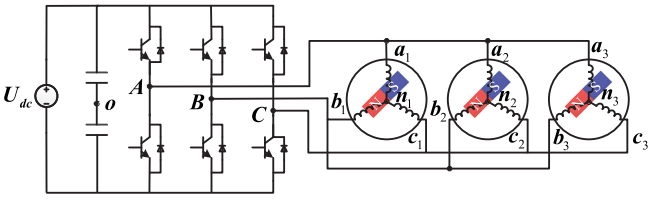

Fig. 2. Mono-inverter driving 3 × 3 phase PMA-SynRM.

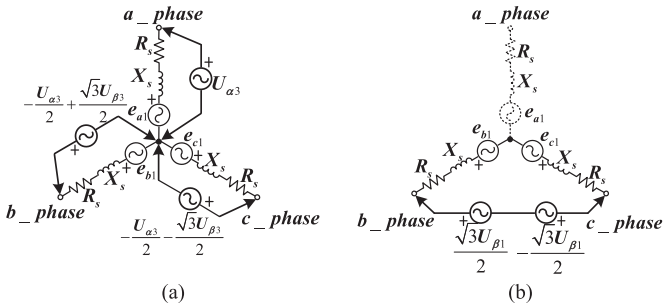

Fig. 3. Equivalent circuit diagrams of the motor. (a) Normal condition. (b) a1-phase open-circuit.

In [32], the electromagnetic torque of the motor is composed of PM torque and reluctance torque, which can be given by

$$\begin{cases} T_{emi} = \dfrac{3}{2} P \psi_f i_{qi} \\ T_{eri} = \dfrac{3}{2} P (L_d - L_q) i_{di} i_{qi} \end{cases} \tag{1}$$

where T_{emi} and T_{eri} are PM torque and reluctance torque, respectively, and subscript $i = 1, 2, 3$ denotes three modules. P is the number of pole pairs of the motor. ψ_f is PM flux linkage, and i_d, i_q, L_d and L_q are currents and inductances in d–q axes, respectively.

In the stationary reference frame, the winding voltage equation can be expressed as

$$\begin{bmatrix} u_{\alpha i} \\ u_{\beta i} \end{bmatrix} = R_s \begin{bmatrix} i_{\alpha i} \\ i_{\beta i} \end{bmatrix} + \omega_r \psi_f \begin{bmatrix} -\sin\theta \\ \cos\theta \end{bmatrix} + L_s(\theta) \begin{bmatrix} \frac{di_{\alpha i}}{dt} \\ \frac{di_{\beta i}}{dt} \end{bmatrix} + \frac{dL_s(\theta)}{dt} \begin{bmatrix} i_{\alpha i} \\ i_{\beta i} \end{bmatrix} \tag{2}$$

where $u_{\alpha i}$, $u_{\beta i}$ and $i_{\alpha i}$, $i_{\beta i}$ are the voltages and currents in α- and β- axis, respectively. R_s is the phase winding resistance. ω_r and θ represent electrical angular speed and electrical angle, respectively. $L_s(\theta)$ is the inductance matrix, which can be denoted as

$$L_s(\theta) = \begin{bmatrix} L_0 + \Delta L \cos 2\theta & \Delta L \sin 2\theta \\ \Delta L \sin 2\theta & L_0 - \Delta L \cos 2\theta \end{bmatrix} \tag{3}$$

where $L_0 = (L_d + L_q)/2$, $\triangle L = (L_d - L_q)/2$.

It should be stressed that since the mutual inductance between modules can be ignored, the inductance of each module is only determined by the self-inductance and mutual inductance of the corresponding module.

III. Modeling Under Different Operation

In this section, the operation conditions of normal and fault of the motor will be introduced. It is worth noting that the torque ripple of the motor is mainly generated by the reluctance torque. The influence of the PM torque ripple can be ignored.

A. Normal Operation

Fig. 3(a) shows the equivalent circuit diagram under normal conditions. According to Kirchhoff's voltage law, the phase currents in steady-state can be calculated as follows:

$$\begin{cases} i_{ai} = \dfrac{u_{\alpha i} - e_{ai}}{R_s} \\ i_{bi} = \dfrac{1}{R_s}\left(-\dfrac{1}{2}u_{\alpha i} + \dfrac{\sqrt{3}u_{\beta i}}{2} - e_{bi}\right) \\ i_{ci} = \dfrac{1}{R_s}\left(-\dfrac{1}{2}u_{\alpha i} - \dfrac{\sqrt{3}u_{\beta i}}{2} - e_{ci}\right) \end{cases} \tag{4}$$

where i_{ai}, i_{bi}, and i_{ci} are phase currents of a-, b-, c-phase, respectively. e_{ai}, e_{bi} and e_{ci} denote back-EMFs of a-, b-, c-phase, respectively.

Because of the parallel connection of the three modules, in normal conditions, the voltages in α- and β- axis applied to each module are the same. In addition, each module shares the same rotational speed and parameters. Therefore, the backEMFs of a-, b-, and c-phase in different modules are equal.

According to the transformation matrix (5), phase current in (4) can be translated into α- and β- axis, as shown in (6)

$$T = \frac{2}{3}\begin{bmatrix} 1 & -\frac{1}{2} & -\frac{1}{2} \\ 0 & \frac{\sqrt{3}}{2} & \frac{\sqrt{3}}{2} \end{bmatrix} \tag{5}$$

$$\begin{cases} i_{\alpha i} = \dfrac{u_{\alpha i} - e_{ai}}{R_s} \\ i_{\beta i} = \dfrac{\sqrt{3}u_{\beta i} - e_{bi} + e_{ci}}{\sqrt{3}R_s}. \end{cases} \tag{6}$$

In order to produce a circular rotating MMF, the current amplitude of $i_{\alpha i}$ should be equal to it of $i_{\beta i}$, and the phase difference is 90°. Therefore, the current equation in the stationary reference frame can also be expressed as

$$\begin{cases} i_{\alpha 1} = i_{\alpha 2} = i_{\alpha 3} = I\cos(\theta + \beta) \\ i_{\beta 1} = i_{\beta 2} = i_{\beta 3} = I\sin(\theta + \beta) \end{cases} \tag{7}$$

where I is the amplitude of phase current and β is the current angle.

In addition, the Park transformation matrix is needed to translate currents from α–β frame to d–q, which can be written as

$$\begin{bmatrix} i_{di} \\ i_{qi} \end{bmatrix} = \begin{bmatrix} \cos\theta & -\sin\theta \\ \sin\theta & \cos\theta \end{bmatrix} \begin{bmatrix} i_{\alpha i} \\ i_{\beta i} \end{bmatrix}. \tag{8}$$

Substituting (7) into (8), the current expression of *d-q* axes can be obtained as

$$\begin{cases} i_{di} = I\cos\beta \\ i_{qi} = I\sin\beta. \end{cases} \tag{9}$$

Finally, applying (9) to (1), the reluctance torque of each module can be given by

$$T_{eri} = \frac{3}{2}P(L_d - L_q)I^2\sin\beta\cos\beta. \tag{10}$$

Since the three modules share the same parameters, the distribution of reluctance torque is uniform. It means that the reluctance torque of each module accounts for 1/3 of the total torque. The parameter *I* can be calculated as

$$I^2 = \frac{T_{eri}}{\frac{3}{2}P(L_d - L_q)\sin\beta\cos\beta}. \tag{11}$$

It should be noted that the parameter *I* can be used to calculate the reference value of the total *d–q* axes currents to realize the closed-loop control of the current. The control accuracy can be affected by different parameters of three modules, but the previous study has verified that the influence is small and can be ignored [11].

B. Fault Operation

In the multiphase motor control system, the possibility of failure will be increased due to the increase in the number of phases. When a fault occurs, the speed and torque of the motor will oscillate. In order to adapt to this degradation condition, the control method should be modified. In this part, a1-phase open-circuit fault is taken as an example to study. The equivalent circuit diagram of a1-phase open-circuit fault is shown in Fig. 3(b). Since the neutral point of the motor is not connected to the midpoint of the dc bus, the zero-sequence current is null and the sum of currents is always zero. It means that the current amplitude of the b1- and c1-phase is equal, and the phase difference is 180°. The phase voltage (u_{kni}, $k = a, b, c, ni$ ($i = 1, 2, 3$) are neutral points of three modules) is equal to the input voltage (u_{mo}, $m = A, B, C$, o is the midpoint of the dc bus) under normal conditions. When an open-circuit fault occurs in one phase, these two voltages will not be equal to each other anymore. Assuming the input voltage is sinusoidal, it can be written as follows:

$$\begin{cases} u_{Ao} = U_m\sin(\theta - \delta) \\ u_{Bo} = U_m\sin(\theta - \delta - 120^\circ) \\ u_{Co} = U_m\sin(\theta - \delta + 120^\circ) \end{cases} \tag{12}$$

where U_m is the amplitude of input voltage and δ is the phase difference between current and voltage.

When a1-phase fails, the voltage of this phase is equal to back-EMF. In addition, the phase voltages of the remaining two phases can be expressed as [33]

$$1M: \begin{cases} u_{bn1} = u_{Bn1} = u_{\mathrm{Bo}} - u_{n1o} = (u_{Bo} - u_{Co})/2 \\ u_{cn1} = u_{Cn1} = u_{\mathrm{Co}} - u_{n1o} = (-u_{Bo} + u_{Co})/2. \end{cases} \tag{13}$$

Applying (12) to (13), phase voltages can be derived as

$$1M: \begin{cases} u_{bn1} = \dfrac{-\sqrt{3}U_m\cos(\theta - \delta)}{2} \\ u_{cn1} = \dfrac{\sqrt{3}U_m\cos(\theta - \delta)}{2}. \end{cases} \tag{14}$$

Since modules II and III operate in normal conditions, the phase voltages are the same. Therefore, these two modules can be regarded as one type. The phase voltages of module II can be described as

$$2M: \begin{cases} u_{an2} = u_{An2} = U_m\sin(\theta - \delta) \\ u_{bn2} = u_{Bn2} = U_m\sin(\theta - \delta - 120^\circ) \\ u_{cn2} = u_{Cn2} = U_m\sin(\theta - \delta + 120^\circ) \end{cases} \tag{15}$$

where 1*M* and 2*M* represent modules I and II, respectively.

By transformation matrix given in (5), the phase voltages in (14) and (15) can be translated into α- and β- axis as

$$1M: u_{\beta 1} = -U_m\cos(\theta - \delta) \tag{16}$$

$$2M: \begin{cases} u_{\alpha 2} = U_m\sin(\theta - \delta) \\ u_{\beta 2} = -U_m\cos(\theta - \delta). \end{cases} \tag{17}$$

According to (12)–(17), it can be concluded that after the failure of phase a1, the voltages of three modules on the β-axis are still the same, which can be expressed as $u_{\beta 1} = u_{\beta 2} = u_{\beta 3}$.

After failure, the phase currents in (4) can be updated as

$$1M: \begin{cases} i_{a1} = 0 \\ i_{b1} = \dfrac{\sqrt{3}u_{\beta 1} - e_{b1} + e_{c1}}{2R_s} \\ i_{c1} = -i_{b1}. \end{cases} \tag{18}$$

It should be emphasized that the phase currents in modules II and III can be obtained through (4) because the fault module has little effect on the normal modules. According to (5), the phase currents in fault and normal modules can be changed as

$$1M: \begin{cases} i_{\alpha 1} = 0 \\ i_{\beta 1} = \dfrac{\sqrt{3}u_{\beta 1} - e_{b1} + e_{c1}}{\sqrt{3}R_s} \end{cases} \tag{19}$$

$$2M: \begin{cases} i_{\alpha 2} = \dfrac{u_{\alpha 2} - e_{a2}}{R_s} \\ i_{\beta 2} = \dfrac{\sqrt{3}u_{\beta 2} - e_{b2} + e_{c2}}{\sqrt{3}R_s}. \end{cases} \tag{20}$$

Since the β-axis voltages and back EMFs of the three modules are the same, according to (19) and (20), it can be seen that the β-axis currents of the three modules are equal. Therefore, the following relationship set up from (12) to (20) can be given by

$$\begin{cases} i_{\alpha 1} = 0, i_{\alpha 2} = i_{\alpha 3} = I_\alpha\cos(\theta + \beta) \\ i_{\beta 1} = i_{\beta 2} = i_{\beta 3} = I_\beta\sin(\theta + \beta) \end{cases} \tag{21}$$

where I_α and I_β are the amplitudes of current in α- and β- axis, respectively.

In order to calculate the reluctance torque of each module, the currents in *d–q* axes based on (8) and (21) are acquired and can

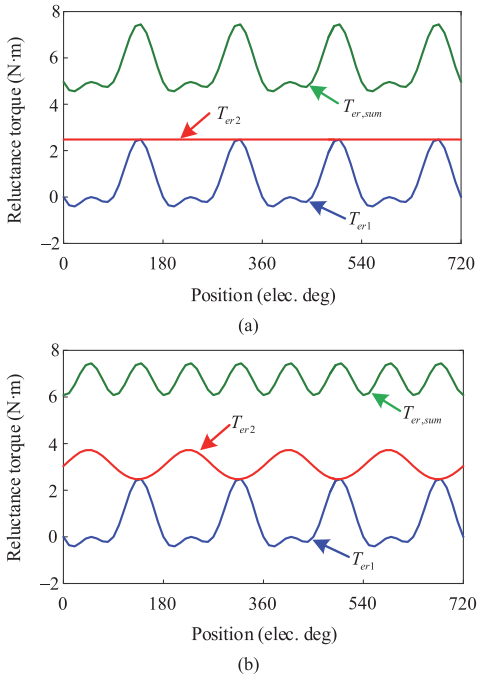

Fig. 4. Reluctance torque of modules I and II under different relationships between I_α and I_β. (a) $I_\alpha = I_\beta$. (b) I_α = sqrt(3/2)I_β.

be expressed as

$$1M: \begin{cases} i_{d1} = I_\beta \sin\theta \sin(\theta+\beta) \\ i_{q1} = I_\beta \cos\theta \sin(\theta+\beta) \end{cases}$$
$$2M: \begin{cases} i_{d2} = I_\alpha \cos\theta \cos(\theta+\beta) + I_\beta \sin\theta \sin(\theta+\beta) \\ i_{q2} = -I_\alpha \sin\theta \cos(\theta+\beta) + I_\beta \cos\theta \sin(\theta+\beta). \end{cases} \tag{22}$$

It can be found that the currents of $d1$-$q1$ will oscillate after the open-circuit fault in a1 when I_β is not equal to zero. In order to minimize the total reluctance torque ripple, the currents in $d2$-$q2$ must also be pulsating, which can be verified from Fig. 4.

Substituting (22) into (1), the total reluctance torque can be given by (23), which is composed of the reluctance torque generated by normal and fault modules

$$\begin{aligned} T_{er,\mathrm{sum}} &= K_t[i_{d1}i_{q1} + i_{d2}i_{q2} + i_{d3}i_{q3}] \\ &= K_t\left[\left(\frac{3}{8}{I_\beta}^2 + \frac{1}{2}I_\alpha I_\beta + \frac{1}{4}{I_\alpha}^2\right)\sin 2\beta \right. \\ &\quad + \left(\frac{3}{4}{I_\beta}^2 - \frac{1}{2}{I_\alpha}^2\right)\sin 2\theta \\ &\quad \left. + \left(-\frac{3}{8}{I_\beta}^2 + \frac{1}{2}I_\alpha I_\beta - \frac{1}{4}{I_\alpha}^2\right)\sin(4\theta+2\beta)\right] \end{aligned} \tag{23}$$

where $K_t = 1.5^* P^*(L_d - L_q)$.

In (23), the average torque and torque ripple can be expressed as

$$T_{er\_\mathrm{avg}} = K_t\left(\frac{3}{8}{I_\beta}^2 + \frac{1}{2}I_\alpha I_\beta + \frac{1}{4}{I_\alpha}^2\right)\sin 2\beta \tag{24}$$

$$\begin{aligned} T_{er\_\mathrm{ripple}} &= K_t\left[\left(\frac{3}{4}{I_\beta}^2 - \frac{1}{2}{I_\alpha}^2\right)\sin 2\theta \right. \\ &\quad \left. + \left(-\frac{3}{8}{I_\beta}^2 + \frac{1}{2}I_\alpha I_\beta - \frac{1}{4}{I_\alpha}^2\right)\sin(4\theta+2\beta)\right]. \end{aligned} \tag{25}$$

Substituting $I_\alpha = I_\beta$ into (23), the total reluctance torque can be expressed as

$$T_{er,\mathrm{sum}}{}' = K_t {I_\beta}^2\left[\frac{9}{8}\sin 2\beta + \frac{1}{4}\sin 2\theta - \frac{1}{8}\sin(4\theta+2\beta)\right]. \tag{26}$$

It means that the total reluctance torque contains second and fourth pulsation components when $I_\alpha = I_\beta$, as shown in Fig. 4(a). The ripple of reluctance torque will be zero in module II, which will increase the total ripple of electromagnetic torque. The ultimate result is that the motor operates in an unstable state. So as to improve the running performance of the motor under failure, configuring I_α and I_β reasonably is very important.

From (24), it can be found that there are one equation and two variables in the system of linear equations, and there are infinite solutions. In previous studies, to obtain the optimal solution of fault-tolerant current, the minimum copper loss is always taken as a constraint condition to reduce the loss of motor after failure [26]. Besides, the minimum torque ripple is also required to ensure the smooth operation of the motor under the fault state. In this part, these two aspects will be introduced, respectively.

1) Minimum Copper Loss: The copper loss can be denoted as

$$\begin{aligned} P_{cu} &= \frac{3}{2}R[{i_{\alpha1}}^2 + {i_{\beta1}}^2 + {i_{\alpha2}}^2 + {i_{\beta2}}^2 + {i_{\alpha3}}^2 + {i_{\beta3}}^2] \\ &= \frac{3}{2}R\left[\left({I_\alpha}^2 + \frac{3{I_\beta}^2}{2}\right) + \left({I_\alpha}^2 - \frac{3{I_\beta}^2}{2}\right)\cos 2(\theta+\beta)\right]. \end{aligned} \tag{27}$$

The currents in the α- and β- axis of different modules can be acquired by using the method of Lagrange multipliers. Taking the minimum copper loss as the objective function, and the average reluctance torque as the constraint condition, the optimal solution of I_α and I_β can be obtained from

$$\begin{aligned} L(I_\alpha, I_\beta, \lambda) &= \left({I_\alpha}^2 + \frac{3{I_\beta}^2}{2}\right) \\ &\quad + \lambda\left[K_t\left(\frac{3}{8}{I_\beta}^2 + \frac{1}{2}I_\alpha I_\beta + \frac{1}{4}{I_\alpha}^2\right)\sin 2\beta - T_{er,avg}\right] \end{aligned} \tag{28}$$

where λ is the Lagrange multiplier. The partial derivatives of (28) give the minimum copper loss condition, which can be expressed as follows

$$\begin{cases} \dfrac{\partial L}{\partial I_\alpha} = 2I_\alpha + \lambda K_t\left(\dfrac{1}{2}I_\beta + \dfrac{1}{2}I_\alpha\right)\sin 2\beta = 0 \\ \dfrac{\partial L}{\partial I_\beta} = 3I_\beta + \lambda K_t\left(\dfrac{3}{4}I_\beta + \dfrac{1}{2}I_\alpha\right)\sin 2\beta = 0 \\ \dfrac{\partial L}{\partial \lambda} = K_t\left(\dfrac{3}{8}{I_\beta}^2 + \dfrac{1}{2}I_\alpha I_\beta + \dfrac{1}{4}{I_\alpha}^2\right)\sin 2\beta - T_{er,\mathrm{avg}} = 0. \end{cases} \tag{29}$$

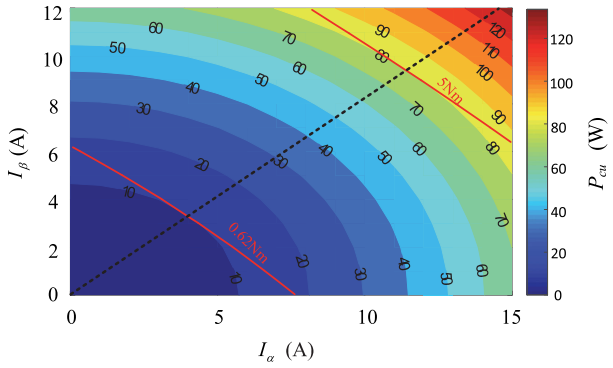

Fig. 5. Contour map of the average copper loss under an a1-phase open-circuit fault.

As a consequence, the relationship between I_α and I_β can be obtained as

$$I_\alpha = \sqrt{\frac{3}{2}} I_\beta. \tag{30}$$

Based on (1), (22), and (30), the mean values of reluctance torque of modules I and II can be expressed as

$$T_{er1\_avg} = K_t {I_\beta}^2 \frac{1}{8} \sin 2\beta \tag{31}$$

$$T_{er2\_avg} = K_t {I_\beta}^2 \left(\frac{5}{16} + \frac{\sqrt{6}}{8} \right) \sin 2\beta. \tag{32}$$

Besides, applying (30) into (24) and (25), the average torque and torque ripple can be updated as

$$T_{er\_avg} = K_t {I_\beta}^2 \left(\frac{3}{4} + \frac{\sqrt{6}}{4} \right) \sin 2\beta \tag{33}$$

$$T_{er\_ripple} = K_t {I_\beta}^2 \left(-\frac{3}{4} + \frac{\sqrt{6}}{4} \right) \sin(4\theta + 2\beta). \tag{34}$$

It means that the reluctance torque contains only the fourth pulsation component when I_α = sqrt(3/2)I_β, which can be seen in Fig. 4(b). According to (31)–(34), it should be noted that T_{er1} = 0.092T_{er} and $T_{er2} = T_{er3}$ = 0.454T_{er}. Therefore, the current amplitude in (11) after the fault can be updated as

$${I_\beta}^2 = \frac{T_{er1\_avg}}{K_t \frac{1}{8} \sin 2\beta}. \tag{35}$$

Fig. 5 shows the contour map of the average copper loss under an a1-phase open-circuit fault. The red solid lines show the torque contour lines under different I_α and I_β, and the torque is 0.62 and 5 N·m, respectively. The tangent point of torque and average copper loss represents the point of maximum torque in the contour line with the same copper loss. The optimal solution can be obtained by connecting all the tangent point, which is shown as the black dotted line in Fig. 5. The relationship between I_α and I_β is sqrt(3/2) in the black dotted line. It means that when I_α = sqrt(3/2)I_β, the minimum copper loss can be achieved under the same load, thus improving the efficiency of the control system.

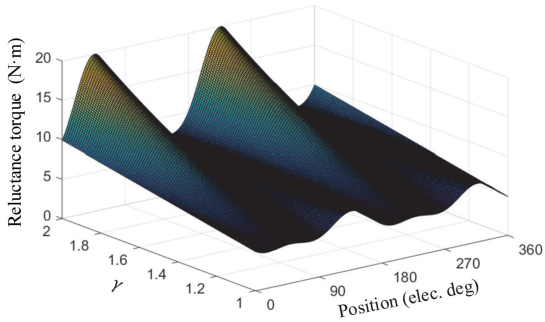

Fig. 6. Relationship between reluctance torque and γ.

2) Minimum Torque Ripple

Assuming that $I_\alpha = \gamma I_\beta$, where γ is the ratio relationship between I_α and I_β. To obtain the minimum torque ripple, it is necessary to minimize the sum of the 2nd and 4th pulsation components in (25). When γ is greater than 2, the ripple of reluctance torque increases with γ. On the contrary, when γ is less than 1, the effect is the opposite. Therefore, the minimum reluctance torque ripple has appeared when γ between 1 and 2. Fig. 6 shows the relationship between reluctance torque and γ. According to the data of Fig. 6, when γ = 1.225, the optimal solution can be obtained. This value is close to the optimal solution in the case of minimum copper loss.

In conclusion, when γ = sqrt(3/2), it cannot only realize the minimum of the reluctance torque ripple but also ensure the minimum of the copper loss. Therefore, taking an a1-phase open-circuit fault as an example, the single-phase FTC strategy has been studied. For other single-phase fault types, it can be transformed into an a1-phase fault only by rotating the reference frame.

C. Controllability Analysis

In this article, the control objects in the current loop are i_d and i_q, those are the sum of the currents in the rotating coordinate system of the three modules. The reference and actual *d*–*q* axes currents can be depicted as

$$\begin{cases} {i_d}^* = 2{I_\alpha}^* \cos(\theta + \beta)\cos\theta + 3{I_\beta}^* \sin(\theta + \beta)\sin\theta \\ {i_q}^* = -2{I_\alpha}^* \cos(\theta + \beta)\sin\theta + 3{I_\beta}^* \sin(\theta + \beta)\cos\theta \end{cases} \tag{36}$$

$$\begin{cases} i_d = 2I_\alpha \cos(\theta + \beta)\cos\theta + 3I_\beta \sin(\theta + \beta)\sin\theta \\ i_q = -2I_\alpha \cos(\theta + \beta)\sin\theta + 3I_\beta \sin(\theta + \beta)\cos\theta \end{cases} \tag{37}$$

where the superscript * indicates the reference value.

The precondition for the stability of the control system is that the actual value can track with the reference, that is to say, (38) needs to be satisfied

$$\begin{cases} {i_d}^* - i_d = 0 \\ {i_q}^* - i_q = 0. \end{cases} \tag{38}$$

According to (36)–(38), the actual I_α can converge to ${I_\alpha}^*$. So, the phase currents can be controlled commendably.

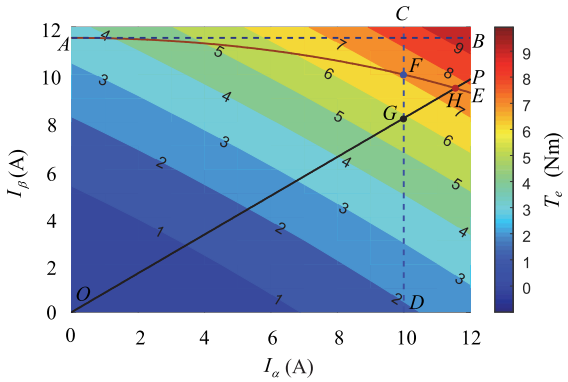

Fig. 7. Contour map of average output torque under a1-phase open-circuit fault.

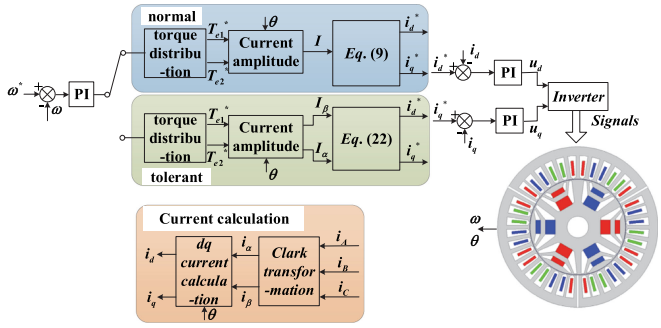

Fig. 8. Block diagram of the control system with mono-inverter.

D. Operating Capability

When an open-circuit fault occurs in the motor under the rated operation condition, the phase current will increase and exceed its rated value. It is dangerous to operate at the phase current higher than the rated value for a long time because it may violate the thermal limits of power electronic converters. Therefore, to achieve the performance of continuous operation after failure, the motor should be derated, that is, operating below the rated value.

$$I_k \le I_{\rm rat}, \forall k \in \{\text{Healthy phases}\} \tag{39}$$

where I_k is the amplitude of phase current, and $I_{\rm rat}$ denotes the rated phase current of the motor.

According to the transformation of (5), the phase currents in (21) can be translated into abc natural frame and can be given by

$$1M: \begin{cases} i_{b1} = \frac{\sqrt{3}}{2} i_{\beta 1} = \frac{\sqrt{3}}{2} I_\beta \sin(\theta+\beta) \\ i_{c1} = -\frac{\sqrt{3}}{2} i_{\beta 1} = -\frac{\sqrt{3}}{2} I_\beta \sin(\theta+\beta) \end{cases} \tag{40}$$

$$2M: \begin{cases} i_{a2} = i_{\alpha 2} = I_\alpha \cos(\theta+\beta) \\ i_{b2} = -\frac{1}{2} i_{\alpha 2} + \frac{\sqrt{3}}{2} i_{\beta 2} = \sqrt{\frac{1}{4}{I_\alpha}^2 + \frac{3}{4}{I_\beta}^2} \sin(\theta+\beta+\zeta_1) \\ i_{c2} = -\frac{1}{2} i_{\alpha 2} - \frac{\sqrt{3}}{2} i_{\beta 2} = \sqrt{\frac{1}{4}{I_\alpha}^2 + \frac{3}{4}{I_\beta}^2} \sin(\theta+\beta+\zeta_2) \end{cases} \tag{41}$$

where ζ_1 and ζ_2 are the phase shift angle.

When an open-circuit fault occurs in phase a1, the maximum value of each phase current of the three modules must satisfy (39). It means that the maximum value of I_α and I_β can be obtained

$$\begin{cases} I_\beta \le I_{\rm rat} \cdot \frac{2}{\sqrt{3}} \\ I_\alpha \le I_{\rm rat} \\ \sqrt{\frac{1}{4}{I_\alpha}^2 + \frac{3}{4}{I_\beta}^2} \le I_{\rm rat}. \end{cases} \tag{42}$$

Fig. 7 shows the contour map of average output torque under a1-phase open-circuit fault. The blue dotted lines AB, CD and dark red solid line AE represent the current limit in the motor, which are all calculated by (42). Therefore, the operation area of the fault-tolerant state needs to be within the AFDO region. According to the analysis in Section III-B, when $I_\alpha =$ sqrt(3/2)I_β, the minimum copper loss and torque ripple can be ensured, which is shown in the black solid line OP. The intersection of black solid line OP and operation area is point G, and the output torque is 5.94 N·m. It means that the maximum output torque is reduced to 66% of the normal state under the condition of ensuring the minimum copper loss and minimum torque ripple. However, if a2- and a3-phase can withstand a certain over-current operation, the maximum output torque can be increased to 84% of the normal state when the operating point G moves to the point H.

IV. Control Strategy

Fig. 8 illustrates the block diagram of the control system, which is controlled by the mono-inverter. The controller consists of normal, tolerant, and current calculation blocks. The fault detection method can be used to judge the operation signatures of the motor [34]. During the presence of phase fault, its characteristics will be displayed in the phase current. Therefore, the method of phase current average values can be used to detect multiple open-circuit failures. Also, to improve the efficiency of the control system, the traditional maximum torque per ampere (MTPA) is used to ensure the minimum copper loss of the motor [35].

As is shown in Fig. 8, a conventional PI controller is used to obtain torque reference value, whose input terminal is the difference between the reference speed and the measured one. The torque of the three modules, which can be used to calculate the amplitudes of phase current, is equal when the motor operates normally. Once an open fault is detected, the program will switch to the fault-tolerant block. The relationship of torque distribution among the three modules needs to be modified according to Section III-B. i_A, i_B, and i_C are the sum of the corresponding phase current of the three modules. The total currents in *d-q* axes are adopted to participate in current closed-loop control. The reference voltage vector in the rotating coordinate system is produced by current controllers, which will take part in space vector pulse width modulation (SVPWM). The voltage signals from the inverter will be sent to the three modules, as shown in Fig. 2.

V. Simulation and Experimental Results

In order to verify the effectiveness of the proposed FTC method, simulations and experiments are accomplished with

TABLE II
PARAMETERS OF 3 × 3 PHASE PMA-SYNRM

Parameters	Value
Pole-pairs	3
Permanent magnet flux linkage	0.01 Wb
Stator resistance	0.202 Ω
D-axis inductance	5.63 mH
Q-axis inductance	17 mH
Rated current	10 A
Rated speed	1600 r/min
Rated torque	9 Nm

TABLE III
TORQUE RIPPLE COMPARISON

	Existing strategy	Proposed strategy
Electromagnetic torque (T_e)	33.32%	20%
Permanent magnet torque (T_{em})	17.97%	27.6%
Reluctance torque (T_{er})	39.48%	22.95%

a 3 × 3 phase PMA-SynRM. The parameters of the motor are given in Table II.

A. Simulation Results

In Fig. 9, the comparisons between the proposed strategy and the existing strategy in [15] are performed to verify the availability of the proposed strategy. The reference speed and load torque are 100 r/min and 4 N·m, respectively. The a1-phase open-circuit fault occurs at 0.6s, and the FTC strategy is adopted at 1.2s. It can be observed that when the fault occurs, the speed starts to fluctuate and the torque ripple is obviously increased. Besides, the current in the fault phase drops to zero, and the phase difference between b1- and c1- phase current is 180°. After 1.2s, the motor operates in fault-tolerant condition, the speed fluctuation and torque ripple are considerably decreased. The torque ripple results are compared in Table III. Since the existing method is to suppress the ripple of PM torque, the influence of reluctance torque ripple is ignored. Therefore, compared to this method, the proposed strategy can effectively suppress the reluctance torque ripple. In addition, the output torque is mainly provided by the reluctance torque in the PMA-SynRM, so the proposed method can significantly reduce the output torque ripple. Besides, for the proposed method, the speed is more stable than the compared method.

Copper losses obtained by these two methods under 4 N·m at fault-tolerant operation are shown in Fig. 10. As can be observed in this figure, the average copper loss of the existing method is 50.17 W, which is 1.1% higher than that of the proposed strategy. Meanwhile, the maximum value of copper loss of the existing method is significantly higher than that of the proposed strategy. Generally, the strategy proposed in this paper has stronger stability and lower copper loss.

Fig. 11 shows the dynamic performances of the proposed control strategy under an a1-phase open-circuit condition when a step variation in load from 5 to 9 N·m and then back to 2 N·m is applied at speed of 100 r/min. It can be noticed that

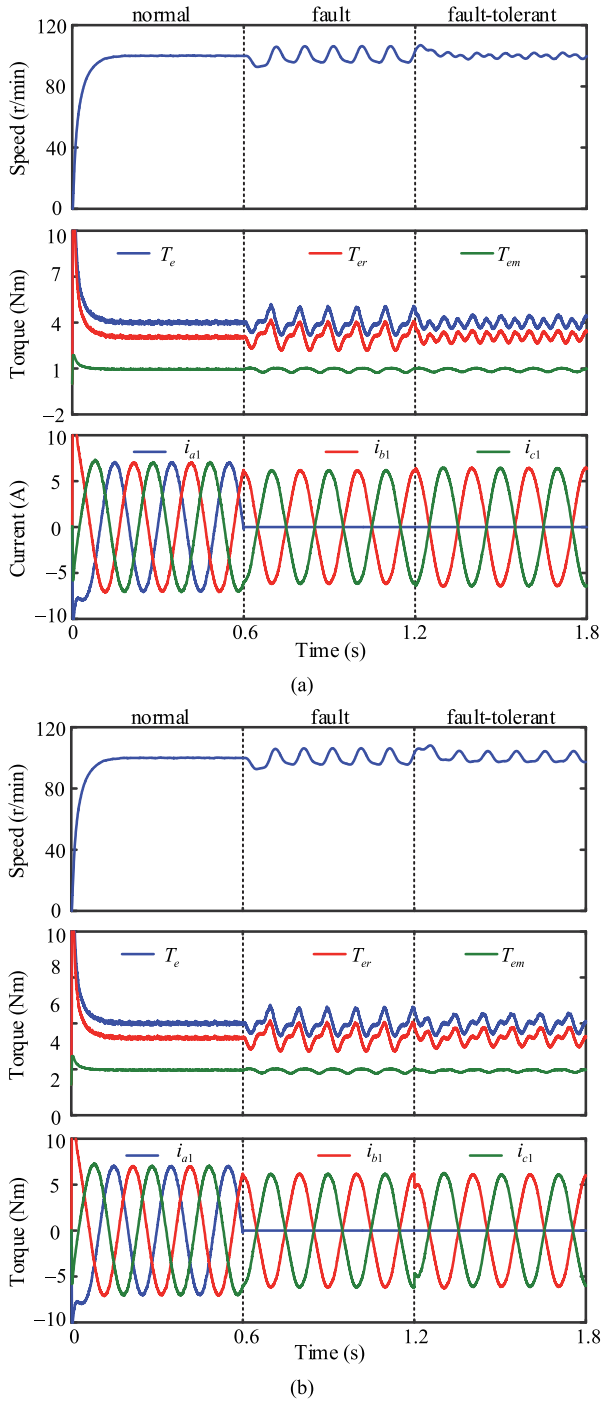

Fig. 9. Simulation waveforms of speed, torque and current under normal, fault and fault-tolerant operations. (a) Proposed strategy. (b) Existing strategy in [15].

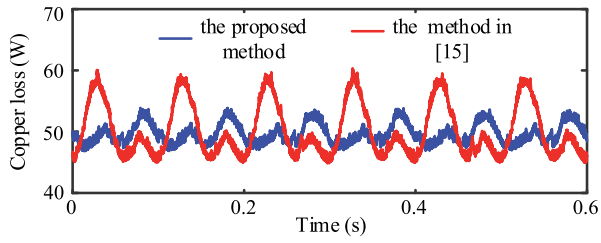

Fig. 10. Comparison of copper loss between the proposed strategy and the existing method.

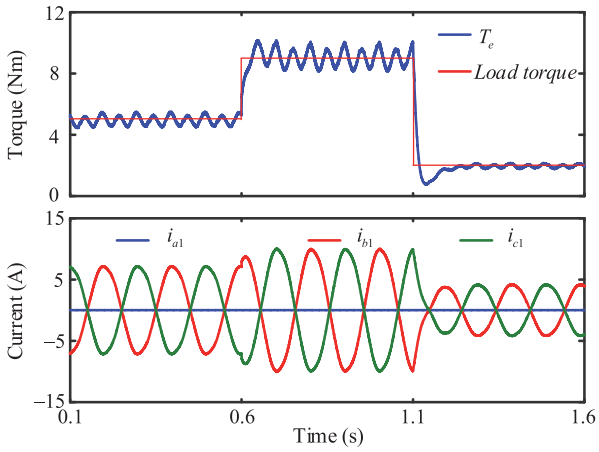

Fig. 11. Simulation waveforms of dynamic performances with 100 r/min under fault-tolerant operation.

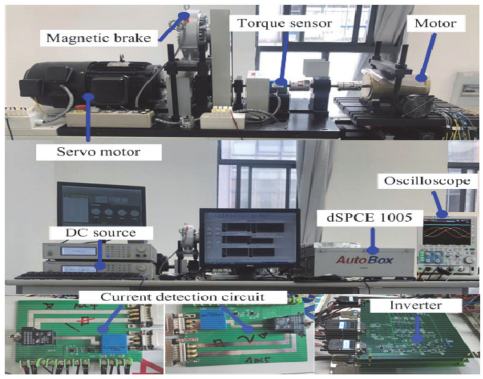

Fig. 12. Experimental setup.

the electromagnetic torque can quickly track the load, which demonstrates that the control system has good robustness.

B. Experimental Results

To further verify the theoretical analysis, the experimental setup of the control system, which consists of a magnetic powder brake as load, dSPACE1005 controller and a two-level three-phase inverter, has been established as shown in Fig. 12. Moreover, the torque is measured by a high precision torque sensor (T20WN/20N·m). An incremental photoelectric encoder is applied to obtain the speed and position. Since the reluctance torque of each module cannot be detected by the torque sensor, in this section, the reluctance torque is obtained by multiplying the torque constant by the *d*–*q* axes currents, as shown in (1). Three current sensors (TA25-NP) are used to detect the total phase current (i_A, i_B, i_C). Furthermore, additional detection circuits are added to detect phase currents in different modules. Due to the limitation of the experimental platform, only 4 additional current sensors are used to detect currents, while the phase currents in module III are not detected. The phase currents detected by current sensors are i_{a1}, i_{b1}, i_{a2}, and i_{b2}, respectively. By detecting the four phase currents, the reluctance torque produced by each module can be calculated. Therefore, this article only

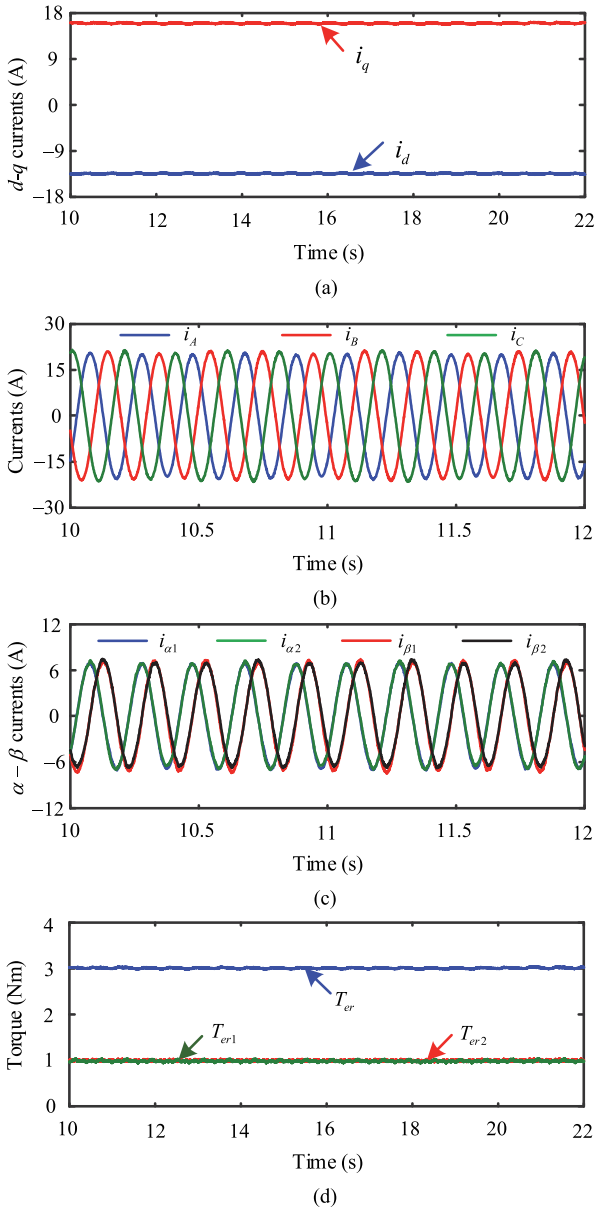

Fig. 13. Experimental results of current and reluctance torque in normal condition at $\omega_{\mathrm{rpm}} = 100$ r/min. (a) *d*- and *q*- axis currents. (b) Sum of phase currents. (c) Stationary α- and β-axis currents. (d) Reluctance torque in modules I, II, and total.

shows the performance of modules I and II. In the process of the experiment, the single-phase open-circuit fault of the motor is simulated by disconnecting one phase deliberately.

The operation performance of the experimental motor driven by the mono-inverter under normal conditions is shown in Fig. 13. The reference speed and load torque of the motor are 100 r/min and 4 N·m, respectively. The total currents in the *d*–*q* axes shown in Fig. 13(a) are constant, which means that the electromagnetic torque is smooth. Since the three modules are connected in parallel and driven by the mono-inverter, the input voltages of the three modules are the same. Therefore, the amplitude of phase current in each module is uniform, and the phase difference between two adjacent phases is 120°, as

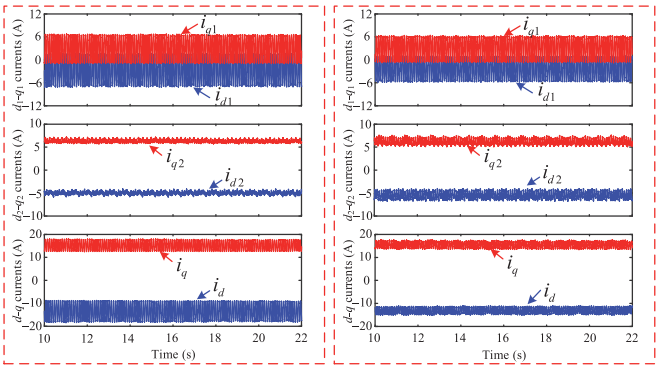

Fig. 14. Experimental waveforms of *d-q* axes current in different modules, without FTC (left) and with the proposed fault-tolerant strategy (right) under one-phase open-circuit.

seen in Fig. 13(b). The waveforms of currents in the α-β coordinate are shown in Fig. 13(c). It should be emphasized that the performance of the three modules is the same in theory, but the difference between the back EMF and the manufacturing process in the experiment cannot be ignored. This is why there are some differences in the currents between the different modules in Fig. 13(c). Besides, the torque ripple of reluctance torque is little in normal condition, which can be seen in Fig. 13(d).

The current waveforms in the *d–q* axes of different modules are shown in Fig. 14. In fault operation (left column), due to a1-phase failure, the pulsation of currents in the rotating coordinate is increased significantly in module I. However, the failure of module I has less influence on modules II and III, so the pulsation of *d–q* axes currents in module II is smaller than it in module I. Besides, the total *d–q* axes currents have a large pulsation in fault operation. After adding the proposed fault-tolerant strategy (right column), the current fluctuations of module II (i_{d2}, i_{q2}) are increased to offset a part of the current fluctuations caused by the fault of module I, thereby reducing the total *d–q* axes current fluctuations.

The waveforms of stator current and reluctance torque of the proposed FTC under a1-phase fault are illustrated in Figs. 15 and 16. From Fig. 15(a), it can be found that, when an open-circuit fault occurs in a1, $i_{\alpha 1} = 0$ can be obtained from the Clark transformation matrix. The phase difference between $i_{\alpha 2}$ and $i_{\beta 2}$ is 90°. In addition, the amplitude of $i_{\alpha 2}$ is higher than it of $i_{\beta 2}$, owing to $I_\alpha = \text{sqrt}(3/2)I_\beta$. It can be seen from Fig. 15(b) that the current amplitude of phase A is lower than it of another phase because the current in a1-phase is equal to zero. The reluctance torque waveforms of different modules are shown in Fig. 16. What calls for special attention is that the reference torque is allocated to normal and faulty modules at a distribution ratio of 45.4% and 9.2%, respectively. The reluctance torque ripple generated by module I mainly contains the second and fourth ripples of the driving frequency, while module II mainly contains the second ripple of the driving frequency. Since the phase difference of the reluctance torque between the modules is approximately 180°, the torque ripple can be suppressed significantly. The experimental results are consistent with the theoretical analysis in Section III.

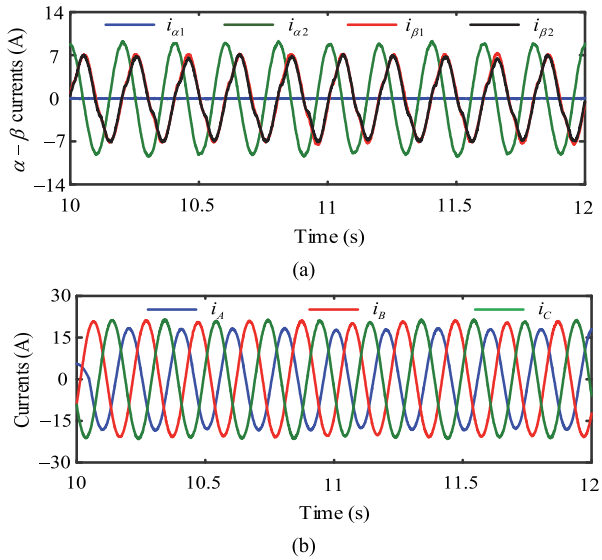

Fig. 15. Experimental waveforms of stator current in (a) stationary α- and β- axis currents and (b) the control phase currents.

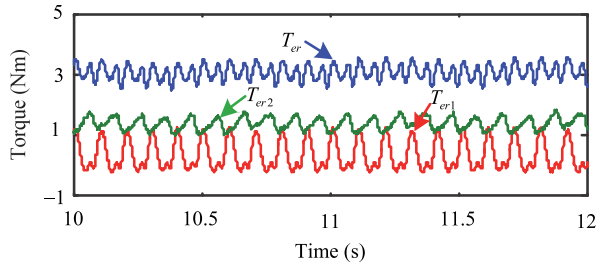

Fig. 16. Experimental results of reluctance torque with the proposed method under one-phase open-circuit.

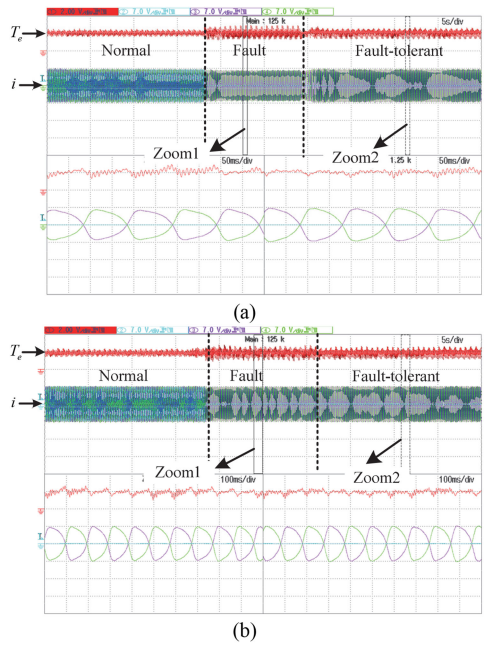

Fig. 17. Experimental waveforms of torque and phase current (i_{a1}, i_{b1}, i_{c1}) under normal, fault, and fault-tolerant operations. (a) Proposed control strategy. (b) Existing method in [15]. T_e is scaled to 4 N·m/div, phase currents are scaled to 7 A/div.

TABLE IV
QUALITATIVE COMPARISON OF CONTROL SYSTEM UNDER THREE DIFFERENT OPERATION MODES

	Normal	Fault	Fault-tolerant
Torque ripple	25%	75%	43.75%
Current THD (i_{b1})	3.84%	18.11%	13.9%
Voltage THD (u_{bn1})	20.3%	53.3%	47.1%
Efficiency	93.3%	80.9%	83%

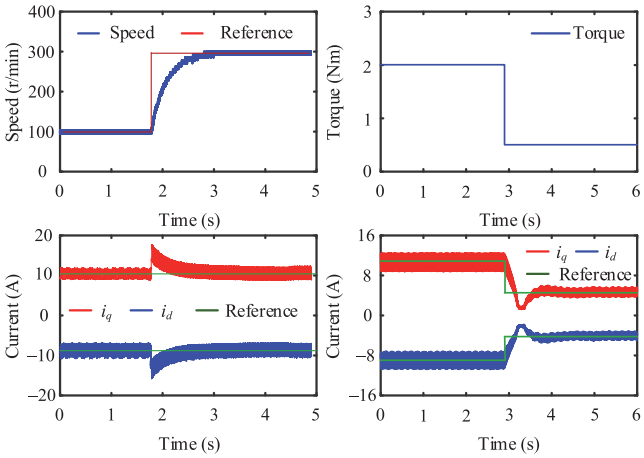

Fig. 18. Dynamic performance of the proposed FTC under a1-phase open-circuit fault.

Fig. 17 shows the experimental waveforms of torque and current under normal, fault, and fault-tolerant operations. The reference speed and load torque of the motor are the same as the above analysis. Zoom1 and Zoom2 are the magnified torque and stator currents in fault and fault-tolerant conditions, respectively. Due to the limitation of the oscilloscope channel, only the stator currents in the module I are collected.

As depicted in Fig. 17(a), the torque and current responses can be used to prove that the motor can run smoothly under normal conditions. However, when a1-phase open-circuit fault occurs, the motor cannot meet the operation requirements owing to the increase of torque ripple. Compared with fault conditions, the torque ripple can be effectively reduced when the proposed FTC strategy is adopted. The pulsation of output torque under fault and fault-tolerant operations is 75% and 43.75%, respectively, which can be given in Table IV. The remaining b1- and c1-phase currents are of the same amplitude and opposite sign since each module has a separated neutral point. Nevertheless, when the method in [15] is applied to FTC, the torque ripple is increased by 19.8% compared with the method proposed in this paper, as shown in Fig. 17(b). As given in Table IV, when the FTC strategy is adopted, the phase current and voltage total harmonic distortions (THDs) are reduced to a certain extent, and the motor efficiency is significantly improved. Therefore, the proposed FTC algorithm driven by the mono-inverter can effectively reduce the torque ripple, thereby improving the stability of the control system.

To evaluate the dynamic performance of the proposed FTC under a1-phase open-circuit fault, the responses of *d–q* currents under speed and torque step are shown in Fig. 18. The reference speed changes from 100 to 300 r/min and the load is 2 N·m (left column). It can be observed that the fast response and low overshoot of speed are realized satisfactorily. In the process of acceleration transient, the *d–q* currents are rapidly modified to provide fast dynamic, while when the speed reaches a steady state, the current remains constant. Besides, as shown in the right column of Fig. 18, the load is varied from 2 to 0.5 N·m, and the reference speed is 100 r/min. The response results show that the *d–q* currents can track the given value quickly. Therefore, the above analysis verifies that the proposed FTC strategy has a good dynamic performance.

VI. CONCLUSION

This article proposed a simple and effective FTC algorithm for a triple redundant 3 × 3 phase PMA SynRM driven by the mono-inverter under a single-phase open-circuit fault. A two-level three-phase inverter has been constructed to drive the parallel-connected motor, which can significantly improve the competitiveness and reduce the complexity of the control system. According to the equivalent circuit diagram, the current relationships among the three modules in the α–β coordinate system after the fault have been analyzed. The Lagrange multiplier method is used to obtain the optimal fault-tolerant current solution in the case of minimum copper loss. In addition, the optimal solution can also achieve the minimum torque ripple. Therefore, the torque can be redistributed by changing the current amplitude of each module to restrain the torque ripple. Because the amplitude of the phase current will be increased after fault tolerance, this limits the output capacity of the motor. However, if a2- and a3- phase can withstand a certain overcurrent operation, the maximum output torque can be increased to 84% of the normal state. The efficiency and reliability of the FTC strategy have been verified by simulation and experimental results. Besides, extending the proposed method into different types of open-circuit faults will be another interesting perspective for future work.

REFERENCES

[1] F. Yu, M. Cheng, and K. T. Chau, "Controllability and performance of a nine-phase FSPM motor under severe five open-phase fault conditions," *IEEE Trans. Energy Convers.*, vol. 31, no. 1, pp. 323–332, Mar. 2016.
[2] J. T. Chen, Z. Q. Zhu, S. Iwasaki, and R. P. Deodhar, "A novel hybrid-excited switched-flux brushless AC machine for EV/HEV applications," *IEEE Trans. Veh. Technol.*, vol. 60, no. 4, pp. 1365–1373, May 2011.
[3] A. Negahdari, A. G. Yepes, J. Doval-Gandoy, and H. A. Toliyat, "Efficiency enhancement of multiphase electric drives at light-load operation considering both converter and stator copper losses," *IEEE Trans. Power Electron.*, vol. 34, no. 2, pp. 1518–1525, Feb. 2019.
[4] V. F. M. B. Melo, C. B. Jacobina, N. Rocha, and E. R. Braga-Filho, "Fault tolerance performance of two hybrid six-phase drive systems under single-phase open-circuit fault operation," *IEEE Trans. Ind. Appl.*, vol. 55, no. 3, pp. 2973–2983, May/Jun. 2019.
[5] R. Gunabalan, P. Sanjeevikumar, F. Blaabjerg, O. Ojo, and V. Subbiah, "Analysis and implementation of parallel connected two-induction motor single-inverter drive by direct vector control for industrial application," *IEEE Trans. Power Electron.*, vol. 30, no. 12, pp. 6472–6475, Dec. 2015.
[6] D. Bidart, M. Pietrzak-David, P. Maussion, and M. Fadel, "Mono inverter multi-parallel permanent magnet synchronous motor: Structure and control strategy," *IET Electr. Power Appl.*, vol. 5, no. 3, pp. 288–294, Mar. 2011.

[7] R. Mai, Y. Chen, Y. Li, Y. Zhang, G. Cao, and Z. He, "Inductive power transfer for massive electric bicycles charging based on hybrid topology switching with a single inverter," *IEEE Trans. Power Electron.*, vol. 32, no. 8, pp. 5897–5906, Aug. 2017.
[8] T. Liu and M. Fadel, "An efficiency-optimal control method for mono-inverter dual-PMSM systems," *IEEE Trans. Ind. Appl.*, vol. 54, no. 2, pp. 1737–1745, Mar./Apr. 2018.
[9] G. Brando, L. Piegari, and I. Spina, "Simplified optimum control method for monoinverter dual parallel PMSM drive," *IEEE Trans. Ind. Electron.*, vol. 65, no. 5, pp. 3763–3771, May 2018.
[10] F. Xu, L. Shi, and Y. Li, "The weighted vector control of speed-irrelevant dual induction motors fed by the single inverter," *IEEE Trans. Power Electron.*, vol. 28, no. 12, pp. 5665–5672, Dec. 2013.
[11] Y. Lee and J. Ha. "Control method for mono inverter dual parallel surface-mounted permanent-magnet synchronous machine drive system," *IEEE Trans. Ind. Electron.*, vol. 62, no. 10, pp. 6096–6107, Oct. 2015.
[12] Z. Deng and X. Nian, "Robust control of two parallel-connected permanent magnet synchronous motors fed by a single inverter," *IET Power Electron,* vol. 9, no. 15, pp. 2833–2845, Aug. 2016.
[13] K. Matsuse, H. Kawai, Y. Kouno, and J. Oikawa, "Characteristics of speed sensorless vector controlled dual induction motor drive connected in parallel fed by a single inverter," *IEEE Trans. Ind. Appl.*, vol. 40, no. 1, pp. 153–161, Jan./Feb. 2004.
[14] M. J. Duran, I. Gonzalez-Prieto, N. Rios-Garcia, and F. Barrero, "A simple, fast, and robust open-phase fault detection technique for six-phase induction motor drives," *IEEE Trans. Power Electron.*, vol. 33, no. 1, pp. 547–557, Jan. 2018.
[15] S. Kwon and J. Ha, "Fault-tolerant operation under single-phase open in mono inverter dual parallel SMPMSM with single shaft," *IEEE Trans. Power Electron.*, vol. 34, no. 12, pp. 12064–12079, Dec. 2019.
[16] X. Jiang, Q. Li, W. Huang, and R. Cao, "A dual-winding fault-tolerant motor drive system based on the redundancy bridge arm," *IEEE Trans. Ind. Electron.*, vol. 66, no. 1, pp. 654–662, Jan. 2019.
[17] U. Choi, F. Blaabjerg, and K. Lee, "Study and handling methods of power IGBT module failures in power electronic converter systems," *IEEE Trans. Power Electron.*, vol. 30, no. 5, pp. 2517–2533, May 2015.
[18] W. Jiabin, K. Atallah, and D. Howe, "Optimal torque control of fault-tolerant permanent magnet brushless machines," *IEEE Trans. Magn.*, vol. 39, no. 5, pp. 2962–2964, Sept. 2003.
[19] A. G. Yepes, J. Doval-Gandoy, F. Baneira, and H. A. Toliyat, "Control strategy for dual three-phase machines with two open phases providing minimum loss in the full torque operation range," *IEEE Trans. Power Electron.*, vol. 33, no. 12, pp. 10044–10050, Dec. 2018.
[20] Y. Sui, P. Zheng, Z. Yin, M. Wang, and C. Wang, "Open-circuit fault-tolerant control of five-phase PM machine based on reconfiguring maximum round magnetomotive force," *IEEE Trans. Ind. Electron.*, vol. 66, no. 1, pp. 48–59, Jan. 2019.
[21] H. S. Che, M. J. Duran, E. Levi, M. Jones, W. Hew, and N. A. Rahim, "Postfault operation of an asymmetrical six-phase induction machine with single and two isolated neutral points," *IEEE Trans. Power Electron.*, vol. 29, no. 10, pp. 5406–5416, Oct. 2014.
[22] H. Zhou, W. Zhao, G. Liu, R. Cheng, and Y. Xie, "Remedial field-oriented control of five-phase fault-tolerant permanent-magnet motor by using reduced-order transformation matrices," *IEEE Trans. Ind. Electron.*, vol. 64, no. 1, pp. 169–178, Jan. 2017.
[23] Q. Chen, W. Zhao, G. Liu, and Z. Lin, "Extension of virtual-signal-injection-based MTPA control for five-phase IPMSM into fault-tolerant operation," *IEEE Trans. Ind. Electron.*, vol. 66, no. 2, pp. 944–955, Feb. 2019.
[24] G. Liu, C. Song, and Q. Chen, "FCS-MPC-based fault-tolerant control of five-phase IPMSM for MTPA operation," *IEEE Trans. Power Electron.*, vol. 35, no. 3, pp. 2882–2894, Mar. 2020.
[25] Z. Changpan, T. Wei, S. Xiang dong, Z. Zhaoji, Y. Guijie, and S. Jianyong, "Control strategy for dual three-phase PMSM based on reduced order mathematical model under fault condition due to open phases," *J. Eng.*, vol. 2018, no. 13, pp. 489–494, Jan. 2018.
[26] M. Shamsi-Nejad, B. Nahid-Mobarakeh, S. Pierfederici, and F. Meibody-Tabar, "Fault tolerant and minimum loss control of double-star synchronous machines under open phase conditions," *IEEE Trans. Ind. Electron.*, vol. 55, no. 5, pp. 1956–1965, May 2008.
[27] A. K. M. Arafat and S. Choi, "Active current harmonic suppression for torque ripple minimization at open-phase faults in a five-phase PMa-SynRM," *IEEE Trans. Ind. Electron.*, vol. 66, no. 2, pp. 922–931, Feb. 2019.
[28] B. Wang, J. Wang, A. Griffo, and B. Sen, "A general modeling technique for a triple redundant 3×3-phase PMA SynRM," *IEEE Trans. Ind. Electron.*, vol. 65, no. 11, pp. 9068–9078, Nov. 2018.
[29] E. B. Sedrine, J. Ojeda, M. Gabsi, and I. Slama-Belkhodja, "Fault-Tolerant control using the GA optimization considering the reluctance torque of a five-phase flux switching machine," *IEEE Trans. Energy Convers.*, vol. 30, no. 3, pp. 927–938, Sept. 2015.
[30] O. Saadeh, M. Dalbah, and Z. Dalala, "Control of two five-phase parallel connected single source motor drives under balanced and unbalanced conditions," in *Proc. 9th IEEE Int. Symp. Power Electron. Distrib. Gener. Syst.*, 2018, pp. 1–6.
[31] B. Wang, J. Wang, A. Griffo, and Y. Shi, "Investigation into fault-tolerant capability of a triple redundant PMA SynRM drive," *IEEE Trans. Power Electron.*, vol. 34, no. 2, pp. 1611–1621, Feb. 2019.
[32] G. Feng, C. Lai, W. Li, J. Tjong, and N. C. Kar, "Open-phase fault modeling and optimized fault-tolerant control of dual three-phase permanent magnet synchronous machines," *IEEE Trans. Power Electron.*, vol. 34, no. 11, pp. 11116–11127, Nov. 2019.
[33] L. Chhun, P. Maussion, M. Pietrzak-David, and M. Fadel, "Analysis of open-phase degradation in a mono-inverter double PMSM system," in *Proc. IEEE Annu. Conf. Ind. Electron. Soc.*, 2011, pp. 486–491.
[34] J. O. Estima and A. J. Marques Cardoso, "A new approach for real-time multiple open-circuit fault diagnosis in voltage-source inverters," *IEEE Trans. Ind. Appl.*, vol. 47, no. 6, pp. 2487–2494, Nov./Dec. 2011.
[35] K. Li and Y. Wang, "Maximum torque per ampere (MTPA) control for IPMSM drives based on a variable-equivalent-parameter MTPA control law," *IEEE Trans. Power Electron.*, vol. 34, no. 7, pp. 7092–7102, Jul. 2019.

Meiling Zhao received the B.Sc. degree in electronic information science and engineering and the M.S. degree in control science and engineering in 2015 and 2018, respectively, from Jiangsu University, Zhenjiang, China, where she is currently working toward the Ph.D. degree in Jiangsu University, Zhenjiang, China.

Her current research interests include multiphase electrical machines and fault-tolerant control.

Guohai Liu (Senior Member, IEEE) received the B.Sc. degree from Jiangsu University, Zhenjiang, China, in 1985, and the M.Sc and Ph.D. degrees in electrical engineering and control engineering.from Southeast University, Nanjing, China, in 1988 and 2002, respectively,

Since 1988, he has been with the Jiangsu University, where since 2002, he has been a Professor with the School of Electrical Information Engineering. He is currently the Director of Jiangsu Key Laboratory of Drive and Intelligent Control for Electric Vehicle. From 2003 to 2004, he was a Visiting Professor with the Department of Electronic and Electrical Engineering, University of Sheffield, Sheffield, U.K. He has authored or co-authored more than 300 technical papers and four textbooks, and is the holder of 80 patents in these areas. His research interests include electrical machines, motor drives for EV and intelligent control.

Dr. Liu is a fellow of Institution of Engineering and Technology (IET), U.K.

Qian Chen (Senior Member, IEEE) received the B.Sc. and Ph.D. degrees from Jiangsu University, Zhenjiang, China, in 2009 and 2015, respectively, in electrical engineering and control engineering.

Since 2015, he has been with Jiangsu University, where he is currently an Associate Professor with the School of Electrical Information Engineering. His current research interests include electric machine design, modeling, fault analysis, and intelligent control.

Wenxiang Zhao (Senior Member, IEEE) received the B.Sc. and M.Sc. degrees from Jiangsu University, Zhenjiang, China, in 1999 and 2003, respectively, and the Ph.D. degree from Southeast University, Nanjing, China, in 2010, all in electrical engineering.

Since 2003, he has been with Jiangsu University, where he is currently a Professor with the School of Electrical Information Engineering. From 2008 to 2009, he was a Research Assistant with the Department of Electrical and Electronic Engineering, University of Hong Kong, Hong Kong. From 2013 to 2014, he was a Visiting Professor with the Department of Electronic and Electrical Engineering, University of Sheffield, Sheffield, U.K He is the author or co-author of more than 110 papers published in various IEEE TRANSACTIONS. His current research interests include electric machine design, modeling, fault analysis, and intelligent control.

Christopher H. T. Lee (Senior Member, IEEE) received the B.Eng. (hons.) and Ph.D. degrees in electrical engineering from the Department of Electrical and Electronic Engineering, The University of Hong Kong, Hong Kong, in 2009 and 2016, respectively.

He is currently an Assistant Professor with the School of Electrical and Electronic Engineering, Nanyang Technological University, Singapore, a Visiting Assistant Professor with the Massachusetts Institute of Technology, Cambridge, MA, USA, and an Honorary Assistant Professor in the alma mater. In these areas, he has authored or coauthored one book, three book chapters, and about 70 referred papers. His research interests include electric machines and drives, renewable energies, and electric vehicle technologies.

Dr. Lee was recipient of many awards, including the NRF Fellowship, the Li Ka Shing Prize (the Best Ph.D. Thesis Prize) and the Croucher Foundation Fellowship.